Journal of Polymers and the Environment (2024) 32:1784–1795
https://doi.org/10.1007/s10924-023-03080-w

ORIGINAL PAPER

Efficient Photocatalytic Degradation of Methyl Red Dye Using Electrospun Nanofibers: A Bio-Inspired Approach for Wastewater Remediation

Jabran Ahmed[1] · Safia Hassan[1] · Muhammad Faiz Ahmad[1] · Zahid Imran[2] · Syed Aminullah[1] · Ayesha Gulzar[1]

Accepted: 3 October 2023 / Published online: 20 October 2023

Abstract

In this study, we investigated the photocatalytic degradation of methyl red dye using Polyvinylpyrrolidone/Tetraethyl orthosilicate (PVP/TEOS) electrospun nanofibers. Which was further calcined at 600°C to synthesis the SiO_2 nanofibers. We analyzed the structural and morphological characteristics of the synthesized nanofibers through various techniques, including Scanning Electron Microscopy (SEM), X-ray diffraction Spectroscopy (XRD), Fourier Transform Infrared spectroscopy (FTIR), and the Brunauer-Emmett-Teller (BET) technique. XRD confirmed the amorphous structure of the nanofibers, while SEM ensured their uniformity and integrity. FTIR analysis indicated the uniform structure of nanofibers. The average nanofiber diameter, calculated using ImageJ software, was approximately 600 nm. We determined the band gap of SiO_2 nanofibers to be 3.16 eV using the Tauc plot method. The degradation of the dye was studied under different conditions, including pH, temperature, dye concentration, and kinetic analysis. The highest degradation of methyl red dye (96%) was achieved at pH 12 and a temperature of 55 °C, with an initial dye concentration of 10 ppm. The kinetic study confirmed the rapid degradation of methyl red dye. Our findings underscore the exceptional effectiveness of SiO_2 nanofibers in dye degradation, attributed to their chemical and biological inertness, as well as biodegradability, achieving a remarkable 96% dye degradation in just 40 min.

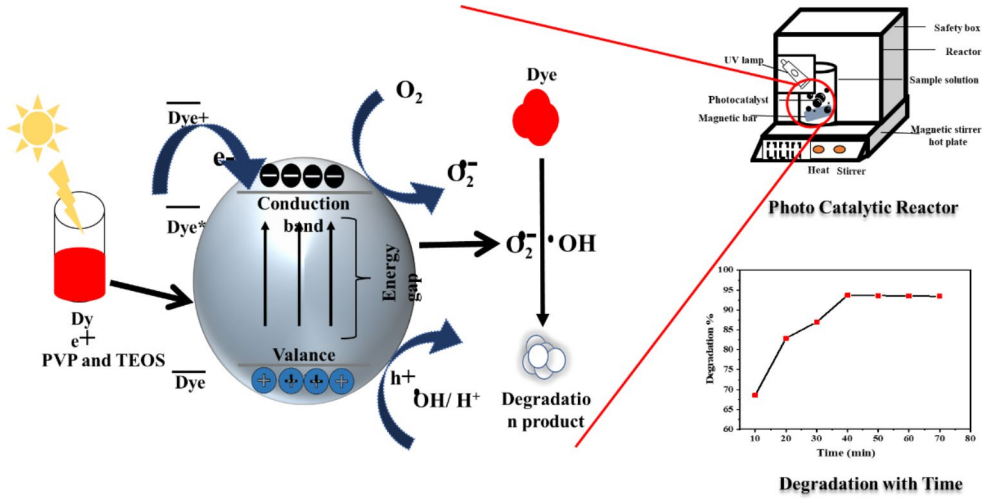

Fig. 1 The graphical abstract represents the mechanism and schematic of the photocatalytic reactor, as well as the dye degradation over time

Introduction

Water is a vital resource for sustainable life, yet anthropogenic activities have led to its degradation [1]. Access to safe drinking water is a cardinal issue globally [2], with

Extended author information available on the last page of the article

Keywords wastewater treatment · electrospun nanofibers · photocatalysis · dye degradation

more than one billion people lacking clean water and 2.5 million requiring water for sanitation [3]. Natural water sources are globally contaminated by pollutants from fertilizer, household, and industrial waste, including organic dyes from various industries [4, 5]. Natural water bodies can experience discoloration due to pollution stemming from residential and industrial activities, where heavy metals, cyanide, nitrogen, toxic organics, phenols, phosphorus, suspended particles, and dyes act as significant contributors to this environmental concern [6]. Millions of tons of untreated dye effluents are discharged annually into natural water bodies worldwide [7]. Even at low concentrations, non-biodegradable, carcinogenic, and harmful dye-contaminated fluids released into the water can cause severe health issues in humans, plants, and animals [8]. Methyl red, an azo dye, is hazardous, causing skin, eye, and digestive irritation. It is a mutagenic, mitotic toxin, and carcinogenic. Its non-biodegradability and toxicity necessitate its removal from wastewater [9].

Dye removal employs various methods: physical approaches like coagulation, filtering, flocculation, and adsorption; chemical techniques like Photocatalysis, Electro-Fenton, and Ozonation; and biological methods such as biodegradation, biosorption, and the use of microbes and enzymes [10, 11]. The photocatalytic degradation of dyes holds great promise as a viable approach to address environmental pollution and effectively remediate dyes from wastewater [12]. At standard temperature and pressure (STP) conditions, photocatalysis presents a feasible alternative for eliminating emerging contaminants through oxidation reactions [13].

Nanofibers exhibit significantly higher photocatalytic activities for photocurrent generation when compared to nanoparticles. This enhanced performance can be attributed to the interparticle connections within the nanofiber network and the presence of a mesoporous structure [14]. One of the cutting-edge methods for producing ultrathin nanofibers is electrospinning [15]. Electrospun nanofibers are vital for wastewater treatment, effectively removing organic and inorganic pollutants. Embracing these techniques reduces reliance on traditional methods, saving materials and energy [16]. We can also synthesize nanofiber membranes to achieve recyclability, improved recovery, and reusability [17].

PVP was preferred for PVP/TEOS nanofiber synthesis due to its high solubility, preventing phase separation, cross-linking ability for thermal stability and mechanical strength, and low scattering loss, beneficial for photo-responsive applications [18]. PVP is a biocompatible polymer known for its non-toxic, inert, pH-stable, and temperature-resistant properties. Additionally, it exhibits biodegradability, making it environmentally friendly [19]. The addition of TEOS into PVP increased the thermal stability of microfibers [20] and TEOS is known for its non-harmful nature and widespread application in biomedical contexts [21]. PVP exhibits excellent solubility in water and various organic solvents, allowing it to interact effectively with a wide range of hydrophilic and hydrophobic materials. On the other hand, TEOS is typically dissolved in water, ethanol, or methanol [20]. SiO_2 composite nanofibers can be easily fabricated through the electrospinning process [22].

A variety of materials have been employed by various researchers in previous studies to degrade methyl red dye. Some examples of these materials are included, along with their degradation times in parentheses. These examples include Cu_2O/ZnO nanocomposite (4 h.) [23], Ricinus communis Activated Charcoal (90 min) [24], Sulfated TiO_2/WO_3 nanocomposite (2 h.) [25], seaweed-mediated zinc oxide nanoparticles (3 h.) [26], $YMnO_3$/CeO_2 composite (4 h.) [27], Pseudomonas aeruginosa (3 days) [28], ZnO/CdS heterostructures [29], and Enterobacter asburiae strain JCM6051 (72 h.) [30].

Although all the previously mentioned materials have been used for methyl red dye degradation, the majority of them exhibited slow degradation rates, ranging from hours to days. Additionally, their degradation efficiency was not satisfactory. In response to this challenge, the study focused on introducing SiO_2 nanofibers as a potential solution. These nanofibers demonstrated exceptional performance in degrading methyl red dye, achieving an impressive 96% degradation efficiency within a mere 40 min.

Experimental Section

Materials

The nanofibers were synthesized using chemicals sourced from Sigma-Aldrich, USA. The chemicals used included Polyvinylpyrrolidone (PVP) with an average molecular weight of 40,000, tetraethyl orthosilicate (TEOS) with a purity of 99%, sodium hydroxide pellets (NaOH) with a purity of $>98\%$, acetic acid glacial (CH_3COOH) with a purity of 99.8%, ethanol (C_2H_5OH) with a molecular weight of 46.07 g/mol, and methyl red with a molecular weight of 269.30 g/mol. Deionized water was used exclusively throughout the synthesis process.

Synthesis of SiO_2 Nanofibers

The electrospinning method was employed to synthesize SiO_2 nanofibers [31, 32]. The apparatus includes a needle, syringe, high voltage supply, vacuum chamber, magnetic hot plate, magnetic stirrer, weigh balance, and conducting substrate. To synthesize PVP/TEOS nanofibers, a solution is prepared by dissolving 3 g of Polyvinyl Pyrrolidone (PVP) in 20 mL of ethanol. In a separate container, a mixture of 10 mL ethanol, 10 mL acetic acid, and 1.5 mL TEOS is prepared. The TEOS mixture is then added dropwise to the PVP solution.

The prepared solution is loaded into a plastic syringe connected to a metallic needle (20 gauge). A voltage of 28 kV is applied across a distance of 14 cm between the needle and the collector. The solution flows from the needle, forming a droplet that is deformed by the applied voltage, creating a cone known as the Taylor cone. A jet is formed when the electrostatic repulsion force overcomes surface tension, and fibers are deposited on a collector covered with aluminum foil. After deposition, the aluminum foil is dried in a microwave oven for 1 h. The fibers are collected from the aluminum foil and transferred to a crucible, which is then placed in a furnace. The fibers are heated at 600 °C for 6 h, resulting in the production of SiO_2 nanofibers.

Characterizations

The identification of major functional groups in the SiO_2 nanofibers was conducted using a Fourier transform infrared (FTIR) spectrophotometer (Spectrum 100, Perkin Elmer) operating in the range of $4000 - 400\ cm^{-1}$. The surface morphology and elemental composition of the adsorbent were examined using scanning electron microscopy (JSM5910, JEOL, Japan). The crystallinity and purity of the SiO_2 nanofibers were determined using a Bruker X-ray diffractometer (model D8 Advance) equipped with Cu-Kα radiation ($\lambda = 1.5405$Å). The specific surface area of the SiO_2 nanofibers was investigated using the BET method [33] at a temperature of -196 °C with the assistance of Quantachrome Autosorb 6B BET equipment.

Adsorption at Different Time Intervals

A 10 ppm stock solution of methyl red was prepared in deionized water. Each vial containing 15 mL of the methyl red stock solution was supplemented with approximately 0.0015 g of the SiO_2 nanofibers sample. The agitation was set at 150 revolutions per minute, and the solutions were agitated for 10, 20, 30, 40, 50, 60, and 70 min at 25 °C. Afterward, the methyl red solution was filtered using filter paper, and the quantity of methyl red adsorbed by the SiO_2 nanofibers was determined by measuring the UV absorbance of the filtrate at 464 nm using a UV-Vis spectrophotometer (UV-1280, SHIMADZU).

Photocatalytic Degradation at Different Times, Concentrations, Temperatures, and pH

The photocatalytic activity of SiO_2 nanofibers was studied by the degradation of methyl red dye. The SiO_2 nanofibers (0.0015 g), containing the adsorbed methyl red dye, were subjected to a UV light source under various experimental conditions. These conditions included different initial concentrations of methyl red (ranging from 10 to 70 ppm), varying exposure times (10 to 70 min), different pH levels (2, 4, 6, 7, 9, and 12), and temperatures (25 °C, 35 °C, and 55 °C). The UV light source utilized had a power of 500 W and emitted light at a wavelength of 380 nm. After exposure to the UV light, the sample was centrifuged at 7000 rpm for 12 min, and the resulting supernatant was analyzed using a UV-visible spectrometer. The UV–visible spectrophotometer was also used to determine the band gap.

The efficiency of methyl red degradation can be assessed using Eq. (1) [34].

$$\frac{C_o - C_t}{C_o} \times 100 \tag{1}$$

where C_o is the initial concentration of MR dye (mg/L) whereas the concentration of MR (C_t) refers to the concentration of MR dye after a fixed interval of time under irradiation.

Determination of Point of Zero Charges (PZC) Value

The solid addition method was employed to determine the point of zero charges (PZC) value of the SiO_2 nanofibers [35]. To achieve this, $NaNO_3$ solutions were prepared with pH values ranging from 1 to 13. These solutions were created using 0.1 mol. L^{-1} NaOH and HCl. Next, 0.05 g of the SiO_2 nanofibers were added to each solution. After allowing 48 h for equilibration, the pH values were recorded. By plotting the difference between the initial and final pH values against the initial pH values, the pHpzc value was determined. The point of zero charges (PZC) was determined by identifying the pH value at which it equals zero, indicating the absence of a net charge [36]. All pH measurements were recorded by using a pH meter (EC700, APERA, USA).

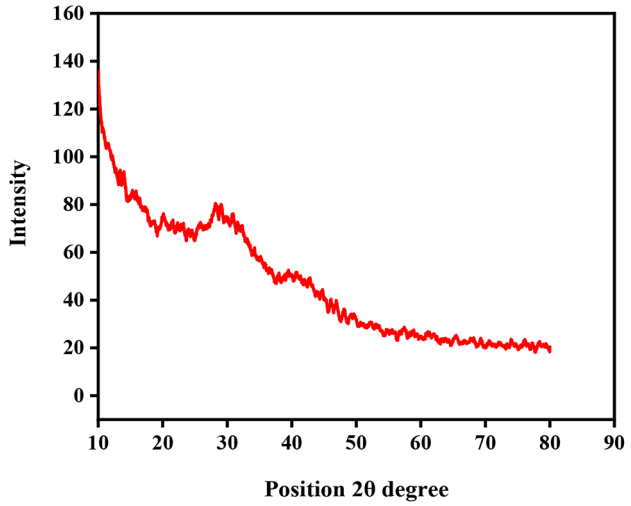

Fig. 2 XRD of synthesized SiO2 nanofibers showing the amorphous nature of nanofibers

Result and Discussion

Characterization

X-Ray Diffraction Analysis (XRD)

The XRD pattern of SiO_2 nanofibers is shown in Fig. 2. The presence of a broad peak spanning the range of 15˚ to 35˚ suggests that SiO_2 nanofibers possess an amorphous structure [37]. In line with previous findings, the PVP nanofibers displayed characteristic peaks at approximately 11° and 21° [38]. However, in the case of the SiO_2 nanofibers, the intensity of the PVP peaks decreased noticeably, and a broad peak emerged at around 25°, which can be attributed to the presence of amorphous O-Si-O bonds within the SiO_2 structure. [39].

Scanning Electron Microscopy (SEM)

Figure 3a and b present SEM images of SiO_2 nanofibers captured at various magnifications. These nanofibers demonstrate an average diameter of approximately 0.5 µm (500 nm) [37]. The synthesized SiO_2 nanofibers remained intact and exhibited a consistent structure. The electrospinning method enabled the production of smooth and non-oriented fibers with micron-sized diameters from a solution of SiO_2 [40].

Fourier Transform Infrared (FT-IR)

Figure 4 displays the FTIR spectrum of the SiO_2 nanofibers. Different well-defined absorption bands can be observed at about 3406, 1640, 1054, 967, and 790 cm^{-1}. The band detected at 3406 cm^{-1} corresponds to the stretching vibration of the O-H bond in water that is adsorbed [20, 41]. The band at 1640 cm^{-1} is related to C = O bonding which indicates the presence of PVP [42, 43]. The absorption band around 1054 cm^{-1}, being the most intense, corresponds to the Si-O asymmetric stretching vibration [44] while Si-O symmetric vibration at about 790 cm^{-1} [20] depicts the presence of SiO_2. The band at 967 cm^{-1} is related to the stretching vibration of the silanol Si-OH group [45].

Brunauer-Emmett-Teller (BET) Study

Figure 5 illustrates the adsorption-desorption curve obtained for the fabricated SiO_2 nanofibers. The SiO_2 nanofibers belong to mesopores as the range of pore size for these nanofibers is between (2–50 nm) [46]. The relative pressure (p/p_o) determines the size of each pore. Specifically, the pore size of the SiO_2 nanofibers measures 6.1 nm, accompanied by a pore volume of 0.11 cm^3/g. The nanofibers' high pore volume and pore area facilitate the binding of ions and molecules to active sites. Moreover, the specific surface area of the SiO_2 nanofibers is significantly high, measuring 53.4 m^2/g. The BJH (Barrett-Joyner-Halenda) adsorption for the SiO_2 nanofibers is 0.13 cm^3/g. By increasing the pore volume in the SiO_2 nanofibers, a larger number of dye molecules can be accommodated, resulting in enhanced adsorption capacity and subsequently increased degradation.

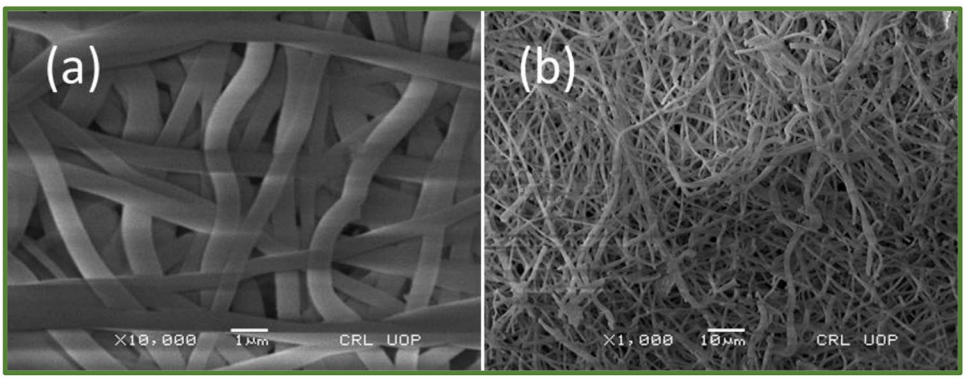

Fig. 3 SEM images of **SiO_2**nanofibers **(a and b)**, depicting the uniform and smooth surface

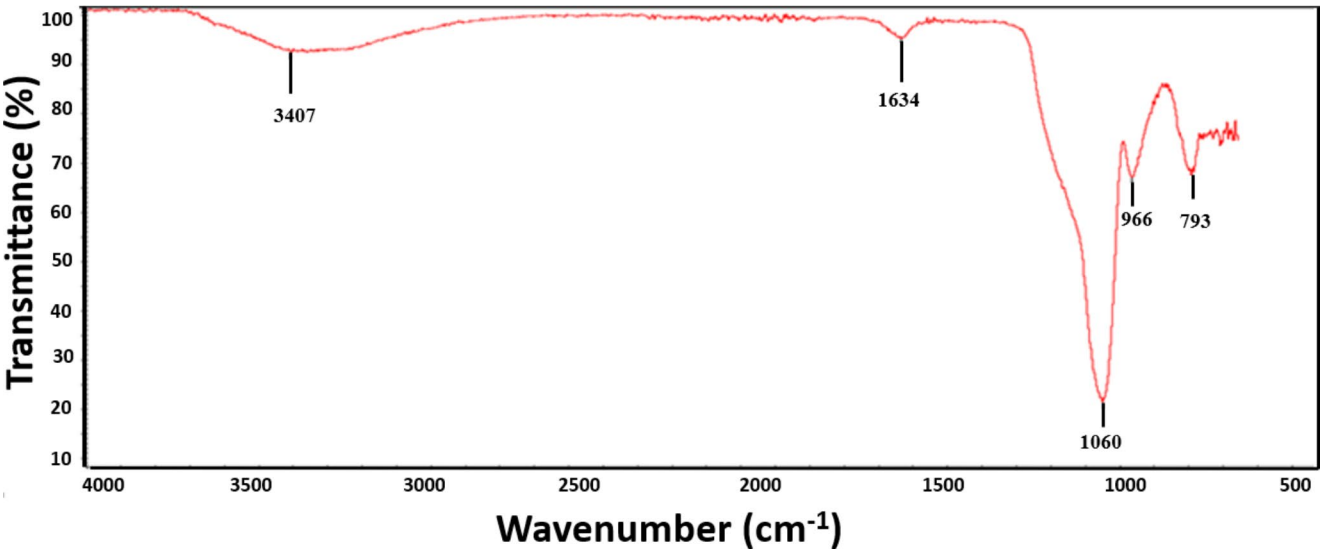

Fig. 4 FTIR spectrum, showing the characteristic absorption bands of SiO_2 nanofibers

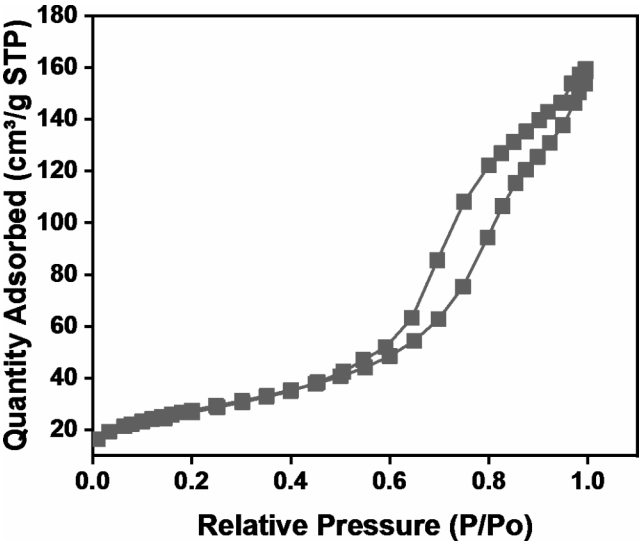

Fig. 5 Adsorption Desorption curve for fabricated SiO_2 nanofibers

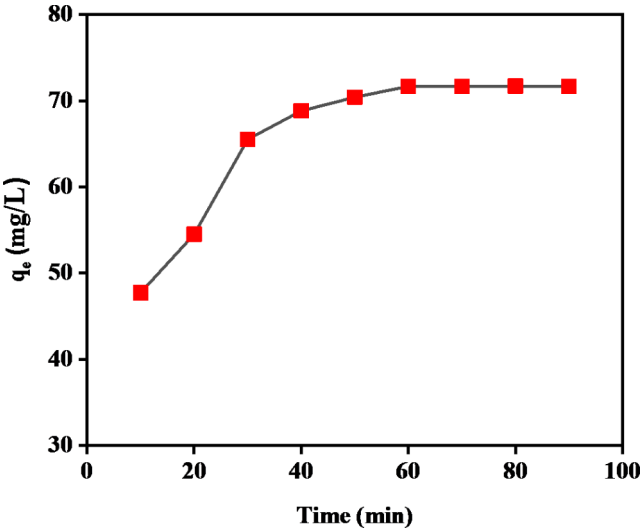

Fig. 6 Adsorption study of Methyl Red at different periods

Raman Spectroscopy

Raman spectroscopy is a potent, non-destructive technique frequently used for analyzing SiO_2 films. Since optical interference greatly influences Raman scattering in thin films, a certain peak's position is directly connected with the thickness of the SiO_2 layer. This large peak in the SiO_2 Raman spectra changes to the low-energy side with a reduction in layer thickness [47]. The main SiO_2 peak is connected to the symmetric stretching of Si-O bonds. It normally appears between 450 and 480 cm^{-1} [48].

Adsorption of MR Dye at Different Time Intervals

The results of the synthesized SiO_2 nanofibers are shown in Fig. 6. It is evident from the trend that SiO_2 nanofibers exhibit significantly faster and more extensive adsorption of methyl red. This accelerated adsorption can be attributed to the presence of a larger number of active sites [49] on the surface of SiO_2 nanofibers. The SiO_2 nanofibers possess an adsorption capacity of approximately 71 mg/L. Over time, the active sites on the adsorbent surface gradually become filled with dye molecules, causing the adsorption rate to slow down. Eventually, an equilibrium stage is reached, and the rate of adsorption becomes constant [50]. The SiO_2 nanofibers achieve equilibrium in just 60 min.

Photocatalytic Study

Band gap Study

The band gap calculation of SiO_2 nanofibers is depicted in Fig. 7, illustrating the energy difference between the highest occupied molecular orbital (HOMO) and the lowest unoccupied molecular orbital (LUMO) states. The calculated band gap for the SiO_2 nanofibers was 3.16 eV. A smaller band gap implies that SiO_2 nanofibers require less energy for electronic transitions, rendering them highly suitable as a catalyst for photocatalytic activities [51].

For the photocatalytic process to occur successfully, the incident light on the catalyst must provide energy equal to or higher than the semiconductor band gap value (eV). This energy was calculated by using Eq. (2) [13].

$$Energy\ (ev)\ = \frac{1239.9}{\lambda} \tag{2}$$

where λ represents the wavelength value. The incident light provided an energy of 3.26 eV, which was greater than the band gap energy of the SiO_2 nanofibers.

Kinetic Study

Figure 8 depicts the photocatalytic degradation of methyl red at 10 ppm, 25°C, natural pH, and different time intervals. The degradation efficiency of SiO_2 nanofibers for methyl red was evaluated over a range of time intervals, ranging from 0 to 90 min. It was observed that SiO_2 nanofibers exhibited a faster degradation of dye molecules, especially during the first 20 min, where they attained 83% dye degradation efficiency. Furthermore, SiO_2 nanofibers reached a maximum degradation efficiency of about 94% in just 40 min [52]. The rapid degradation of the dye can be attributed to the abundance of active sites on the catalyst's surface, which facilitate the adsorption of dye molecules. As time progresses, the active sites on the catalyst surface gradually fill up with dye molecules, leading to a slowdown in the rate of photocatalytic degradation. Eventually, an equilibrium stage is reached, and the degradation rate becomes constant [53].

The Scavenger Effect

In the study, t-butyl alcohol, citric acid, and ascorbic acid served as the scavengers of hydroxyl radicals (•OH), holes (h^+), and superoxide radicals ($\bullet O_2$). The addition of t-butyl alcohol and citric acid to the reaction system (Fig. 9) did not significantly alter the photocatalytic efficiency, the inclusion of ascorbic acid caused a substantial decrease in reaction speed. However, when ascorbic acid was included in the reaction system, the photocatalytic efficiency for MR dropped from 92.1 to 41.4%.

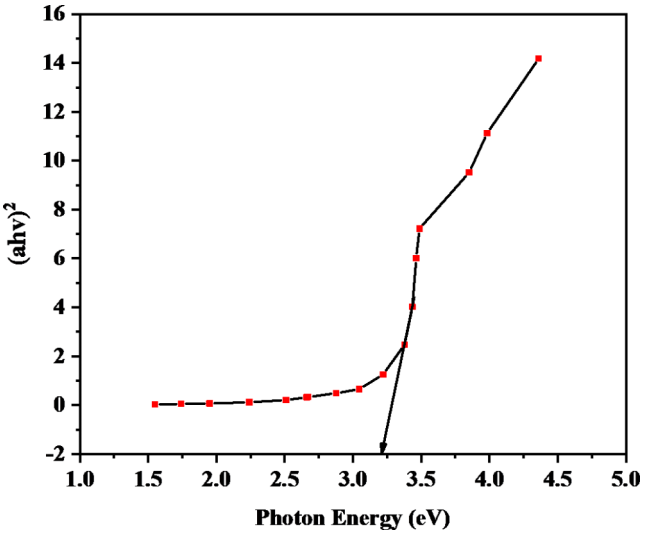

Fig. 7 Tauc plot for SiO_2 nanofibers

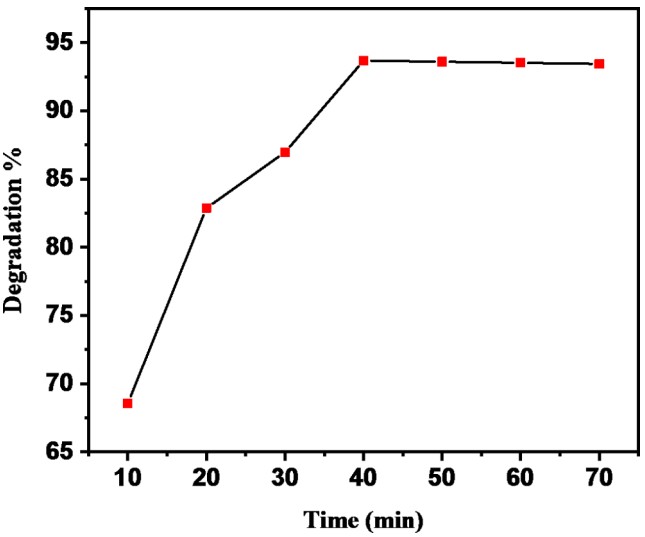

Fig. 8 Photocatalytic Degradation of Methyl Red at different period

Effect of pH of the Solution

pH is a crucial parameter for dye pollutant degradation with a photocatalyst [54]. pH significantly affects adsorption capacity and subsequently the degradation efficiency due to its influence on the surface charge of the adsorbent and the ionization state of dye molecules [55]. The repulsion between methyl red and the SiO_2 composite in acidic conditions can be attributed to the positive charges present on both entities. In an acidic medium, methyl red assumes a quinoid structure with a positive charge, as depicted in Fig. 10(a). Conversely, Fig. 10(b) shows the structure of SiO_2 nanofibers [20], where the nitrogen atom of nanofibers

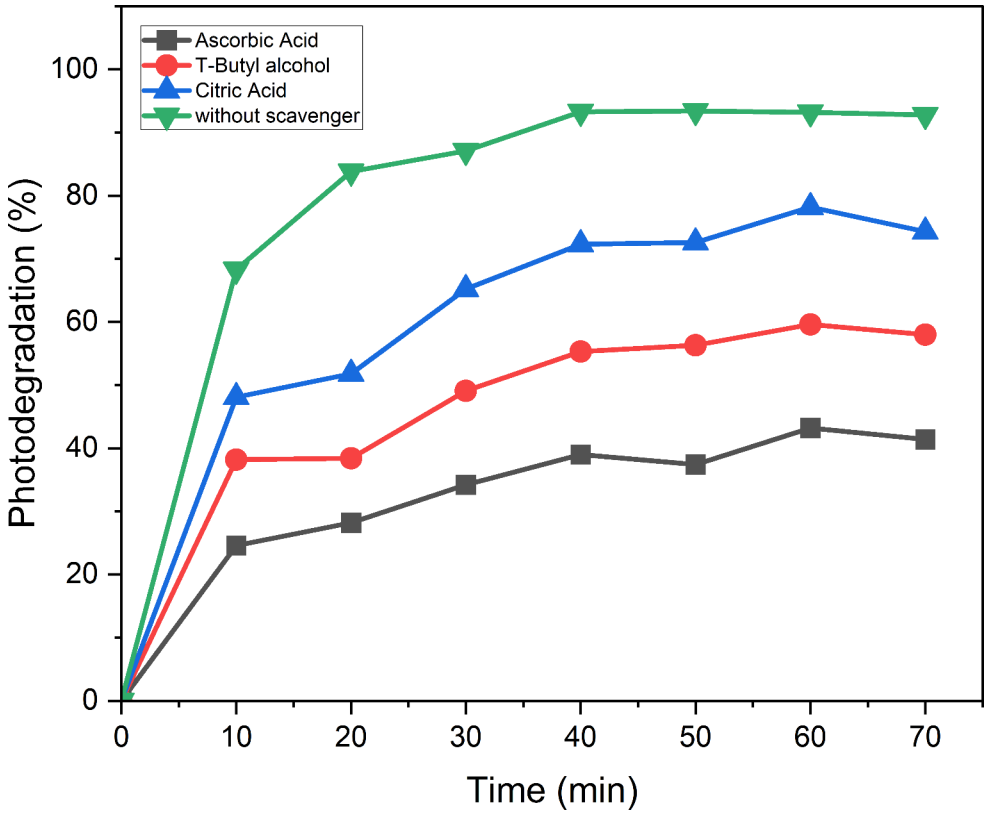

Fig. 9 Effect of several scavengers t-butyl alcohol, citric acid, and ascorbic acid on the photocatalytic degradation of MR.

carries a positive charge. When two positively charged species come into proximity, there is a strong electrostatic repulsion between them. This electrostatic repulsion hinders the adsorption of methyl red onto the surface of the SiO_2 nanofibers, leading to a decreased adsorption capacity and consequently reduced photocatalytic activity in acidic environments. Therefore, the positive charge on both methyl red and the nanofibers creates a barrier to effective adsorption and photocatalysis in acidic conditions.

In Fig. 10(c), the degradation efficiency of SiO_2 nanofibers is shown at various pH levels. The efficiency of degradation is lower in acidic mediums due to the repulsion between methyl red dye and SiO_2 nanofibers. However, at pH 7, the degradation efficiency reached approximately 92%. Interestingly, at pH 12, the maximum degradation efficiency was observed, reaching about 95%. The results indicate that the nanofibers exhibit enhanced degradation performance under alkaline conditions. Typically, dye degradation is commonly accomplished within the alkaline pH range of 6 to 10 [28].

The point of zero charges (pzc) holds great significance in surface science as it governs the substrate's capacity to adsorb potentially harmful ions. In the case of the prepared SiO_2 nanofibers, Fig. 10(d) presents the examination and depiction of the pzc value. The pzc value of the SiO_2 nanofibers was measured at pH 7.1, indicating that the surface of the SiO_2 nanofibers becomes electrically neutral at this pH level [36, 56].

Effect of Initial Dye Concentration

Figure 11(a) shows the effect of initial methyl red concentration at 25°C and natural pH. The degradation of methyl red dye using SiO_2 nanofibers was high at low ppm concentrations, but it decreased at high ppm concentrations. The highest degradation percentage, about 88%, was observed at 10 ppm, while the lowest, only about 5%, was at 70 ppm. The observed decrease in degradation efficiency at higher methyl red concentrations can be attributed to the limited number of active sites available on the SiO_2 nanofibers' surface. When the initial concentration of methyl red is low, there are relatively fewer dye molecules in the solution, allowing for a higher proportion of them to come into contact with and be adsorbed by the available active sites on the nanofibers. Consequently, the degradation percentage is higher at lower concentrations. However, as the initial concentration increases, the active sites may become saturated, resulting in reduced adsorption and, subsequently, lower degradation efficiency at higher ppm concentrations [57].

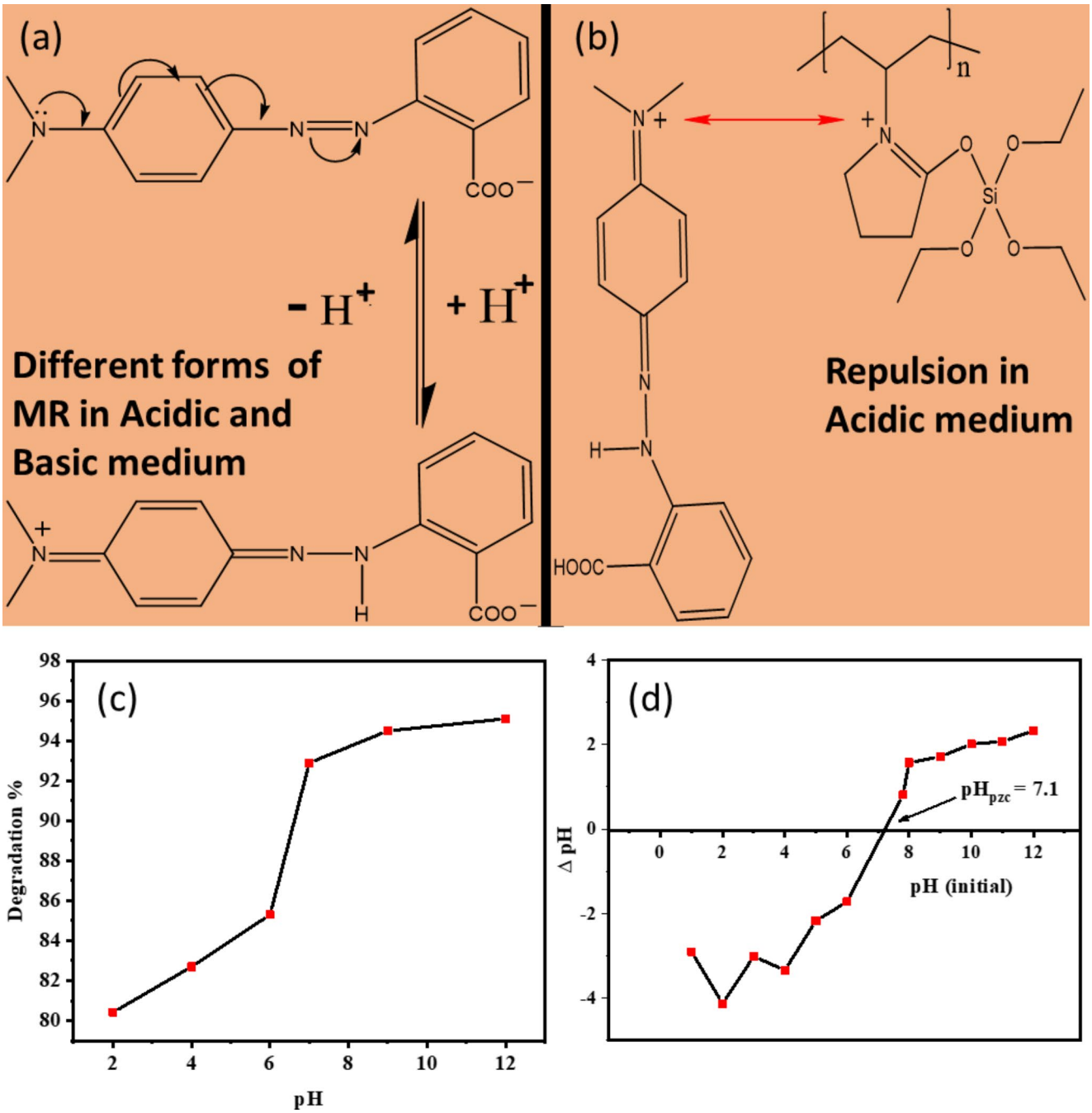

Fig. 10 **(a)** Different forms of methyl red in acidic and basic environments, **(b)** Repulsion between nanofibers and methyl red dye in acidic medium, **(c)** Degradation efficiency of SiO_2 nanofibers at different pH, **(d)** pzc value for the fabricated SiO_2 nanofibers

Effect of Temperature

Figure 11(b) demonstrates the impact of temperature on methyl red degradation at natural pH and constant contact time. The degradation of methyl red dye using SiO_2 nanofibers is high at low temperatures, while it is low at high temperatures. When the temperature was increased from 25 to 55 °C, the degradation decreased from about 95–83%, respectively. The degradation of methyl red dye might involve a specific enzymatic or surface adsorption process. At low temperatures, the nanofibers' surface may be more favorable for the binding and degradation of the dye molecules, leading to a higher degradation efficiency. However, as the temperature is raised, the binding affinity between the nanofibers and the dye may decrease, or the active sites on the nanofibers' surface could change, affecting the efficiency of the degradation process. This could result in a lower degradation percentage at higher temperatures.

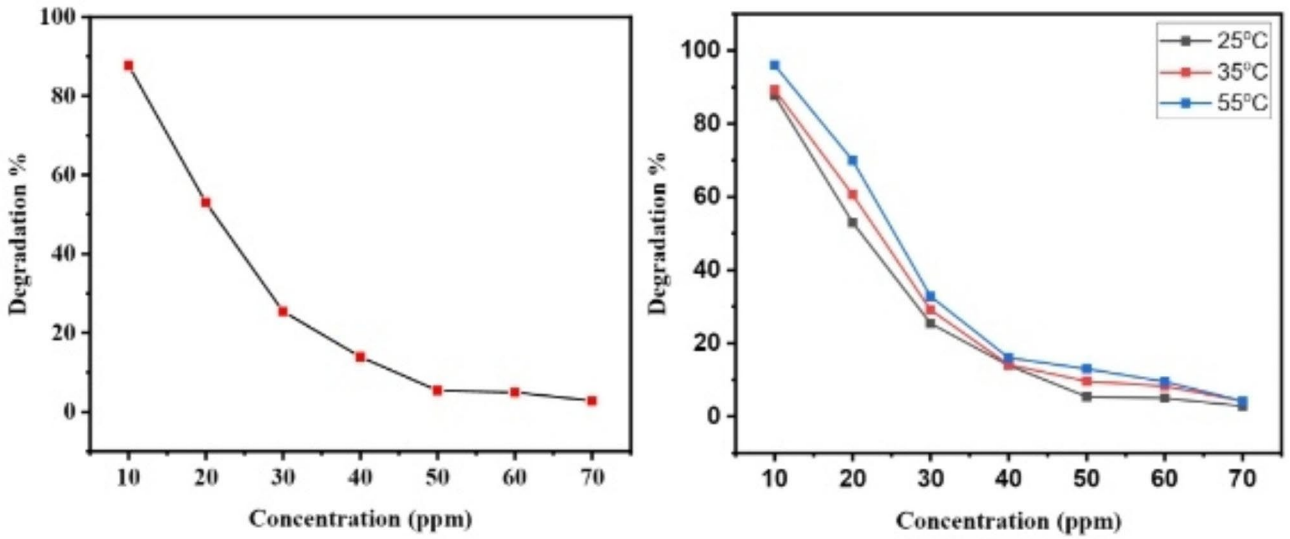

Fig. 11 (a) Methyl Red dye degradation at different concentrations using SiO_2 nanofibers (b) Methyl Red dye degradation at different temperatures using SiO_2 nanofibers

Table 1 Equilibrium Time and Degradation Efficiency of Methyl Red Degradation on SiO_2 Nanofibers Compared to Previous Photocatalysts

Sr.	Material	Degradation Time	Degradation Percentage	Reference
1	Cu_2O/ZnO nanocomposite	4 h	70%	[23]
2	Ricinus communis Activated Charcoal	90 min	82.79%	[24]
3	Sulfated TiO_2/WO_3 nanocomposite	2 h	90%	[25]
4	seaweed mediated zinc oxide nanoparticles	3 h	92%	[26]
5	$YMnO_3$/CeO_2 composite	4 h	45%	[27]
6	Pseudomonas aeruginosa	3 days	88.37%	[28]
7	ZnO/CdS heterostructures		95%	[29]
8	Enterobacter asburiae strain JCM6051	72 h	74.28%	[30]
9	**SiO_2nanofibers**	**40 min**	**96%**	**Present Work**

Comparison

The comparison of present work is compared with the published work shown in Table 1.

Conclusions

In conclusion, this study demonstrates the successful utilization of SiO_2 electrospun nanofibers as highly efficient photocatalysts for the degradation of methyl red dye from wastewater. The nanofibers exhibit a uniform, smooth, and amorphous structure, as evidenced by various characterization techniques. Various characterization techniques were employed to verify the structure and formation of the nanofibers.

By systematically exploring different parameters, such as pH, temperature, and dye concentration, the study identified the optimal conditions for achieving the highest dye degradation efficiency of 96%. Notably, this remarkable level of degradation was attained at a pH of 12 and a temperature of 55 °C, with an initial dye concentration of 10 ppm, within a short duration of 40 min. The exceptional photocatalytic performance of SiO_2 nanofibers is attributed to their chemical and biological inertness, along with their biodegradability, making them environmentally friendly and effective in wastewater treatment processes. Overall, these findings underscore the significant potential of SiO_2 nanofibers as a promising solution for the removal of harmful dye pollutants from natural water sources, offering a pathway toward sustainable water management and pollution mitigation.

Future Recommendations

Further research can focus on optimizing the composition of SiO_2 nanofibers to enhance their photocatalytic efficiency. To evaluate the practical feasibility of SiO_2 nanofibers in wastewater treatment, scaling up the synthesis process is crucial. Large-scale production and testing of these nanofibers under real-world conditions would provide valuable insights into their potential application in industrial settings for the efficient removal of harmful pollutants.

Acknowledgements We acknowledge the COMSATS University Islamabad, Islamabad Campus.

Author Contributions Jibran Ahmed and Muhammad Faiz Ahmad: Designing of experiment, synthesis of material and writing, Aysha Gulzar and Syed Aminullah: Characterization and analysis of the material , Zahid Imran: Figures, review and formal analysis, Safia Hassan: Methodology Conceptualization, Writing editing and review, Supervision.

Funding Information COMSATS University will found the mention manuscript research work.

Declarations

Conflict of interest The authors declare that they have no competing interests that can influence the work reported in this research paper.

References

1. Mishra R, Studies A (2023) *Fresh water availability and its global challenge* 4(3): p. 1–78. https://doi.org/10.37745/bjmas.2022.0208
2. Khashij M et al (2016) *Modeling of the adsorption breakthrough behaviors of 4-chlorophenol in a fixed bed of nano graphene oxide adsorbent*. 65(2): p. 127–134. https://doi.org/10.2166/aqua.2015.077
3. Saravanan A et al (2022) *Experimental studies and analysis on the treatment of groundwater using solar and wind energy*. 15(3). https://doi.org/10.31788/RJC.2022.1536955
4. Preethi PS et al (2022) *Advances in bioremediation of emerging contaminants from industrial wastewater by oxidoreductase enzymes* 359: p. 127444. https://doi.org/10.1016/j.biortech.2022.127444
5. Hasanpour M, Motahari S, Jing D, Hatami MJC (2021) *Investigation of operation parameters on the removal efficiency of methyl orange pollutant by cellulose/zinc oxide hybrid aerogel*. 284: p. 131320. https://doi.org/10.1016/j.chemosphere.2021.131320
6. Alsukaibi AKJP (2022) *Various approaches for the detoxification of toxic dyes in wastewater* 10(10): p. 1968. https://doi.org/10.3390/pr10101968
7. Saxena A, Gupta S (2022) Toxicological impact of Azo Dyes Azo dyes and their Microbial degraded Byproducts on Flora and Fauna. Innovations in environmental biotechnology. Springer, pp 319–343. https://doi.org/10.1007/978-981-16-4445-0_14
8. Ahmad MF et al (2023) *Green Approach to Water Purification: Investigating Methyl Orange Dye Adsorption Using Chitosan/Polyethylene Glycol Composite Membrane* : p. 1–19. https://doi.org/10.1007/s10924-023-02994-9
9. Neolaka YA et al (2023) *Adsorption of methyl red from aqueous solution using Bali cow bones (Bos javanicus domesticus) hydrochar powder*. 17: p. 100824. https://doi.org/10.1016/j.rineng.2022.100824
10. Bal G, Thakur AJMTP (2022) *Distinct approaches of removal of dyes from wastewater: a review*. 50: p. 1575–1579. https://doi.org/10.1016/j.matpr.2021.09.119
11. Hasanpour M, Motahari S, Jing D, Hatami MJAJoC (2021) *Statistical analysis and optimization of photodegradation efficiency of methyl orange from aqueous solution using cellulose/zinc oxide hybrid aerogel by response surface methodology (RSM)*. 14(11): p. 103401. https://doi.org/10.1016/j.arabjc.2021.103401
12. Khalid N, Kalsoom U, Ahsan Z, M.J.I.J.o.B M, Bilal (2022) *Non-magnetic and magnetically responsive support materials immobilized peroxidases for biocatalytic degradation of emerging dye pollutants—A review* 207: p. 387–401. https://doi.org/10.1016/j.ijbiomac.2022.03.035
13. Ruiz Santoyo V et al (2022) *Use of nanostructured photocatalysts for dye degradation: a review*https://doi.org/10.3311/PPch.18885
14. Sahoo B, Panda P, Ramakrishna SJOC (2022) *Electrospinning of functional ceramic nanofibers* : p. 100291. https://doi.org/10.1016/j.oceram.2022.100291
15. Chinnappan BA, Krishnaswamy M, Xu H, Hoque MEJP (2022) Electrospinning of Biomedical nanofibers/nanomembranes: Effects of Process Parameters 14(18):3719. https://doi.org/10.3390/polym14183719
16. Nayl AA et al (2022) *Review of the recent advances in electrospun nanofibers applications in water purification*. 14(8): p. 1594. https://doi.org/10.3390/polym14081594
17. Chabalala MB et al (2021) *Photocatalytic nanofiber membranes for the degradation of micropollutants and their antimicrobial activity: recent advances and future prospects*. 11(9): p. 678. https://doi.org/10.3390/membranes11090678
18. Rahmanian V et al (2023) *Mechanically robust, thermally insulating and photo-responsive aerogels designed from sol-gel electrospun PVP-TiO2 nanofibers*. 32: p. 101784. https://doi.org/10.1016/j.apmt.2023.101784
19. Kurakula M (2020) G.K.J.J.o.d.d.s. Rao, and technology, *Pharmaceutical assessment of polyvinylpyrrolidone (PVP): as excipient from conventional to controlled delivery systems with a spotlight on COVID-19 inhibition*. 60: p. 102046. https://doi.org/10.1016/j.jddst.2020.102046
20. Bramanti E et al (2022) *Structural characterization of electrospun tetraethylortosilicate (TEOS)/Polyvinylpyrrolidone (PVP) microfibres*. 287: p. 126248. https://doi.org/10.1016/j.matchemphys.2022.126248
21. Butt A et al (2019) *Controlled release of cephradine by biopolymers based target specific crosslinked hydrogels* 121: p. 104–112. https://doi.org/10.1016/j.ijbiomac.2018.10.018
22. Zhang X et al (2023) *A novel approach to directly achieve SiO2 hollow nanofibers via mono-axis electrospinning united with fluorination technique*. 330: p. 133307. https://doi.org/10.1016/j.matlet.2022.133307
23. Gaim YT, Tesfamariam GM, Nigussie GY, E.J.J.o.C M (2019) *Synthesis, characterization and photocatalytic activity of N-doped Cu2O/ZnO nanocomposite on degradation of methyl red*. 3(4): p. 93. https://doi.org/10.3390/jcs3040093
24. Abdolhosseinzadeh S, Heier J, Zhang CJ (2020) Printing and coating MXenes for electrochemical energy storage devices. J Physics: Energy 2(3):031004. https://doi.org/10.1016/j.cscee.2022.100287
25. Patil S et al (2019) *Sulfated TiO2/WO3 nanocomposite: an efficient photocatalyst for degradation of Congo red and methyl red dyes under visible light irradiation*. 225: p. 247–255. https://doi.org/10.1016/j.matchemphys.2018.12.041
26. Anjali K et al (2022) *Photocatalytic degradation of methyl red using seaweed mediated zinc oxide nanoparticles*. 43: p. 102384. https://doi.org/10.1016/j.bcab.2022.102384
27. Wang Y, Tian HJO (2020) *Study on the construction of YMnO3/CeO2 composite photocatalyst heterostructure and photocatalytic degradation of methyl red*. 201: p. 163524. https://doi.org/10.1016/j.ijleo.2019.163524
28. Ikram M et al (2022) *Biodegradation of azo dye methyl red by pseudomonas aeruginosa: optimization of process conditions*. 19(16): p. 9962. https://doi.org/10.3390/ijerph19169962
29. Goswami Y, Kaundal JB (2023) S. Begzaad, and R.J.J.o.t.I.C.S. Tiwari, *photocatalytic degradation of Methyl Red dye using highly efficient ZnO/CdS hierarchical heterostructures under white LED*. : p. 1–17. https://doi.org/10.1007/s13738-023-02789-8
30. Singh PJJoAB, Biotechnology (2022) *Bioremediation of hazardous azo dye methyl red by a newly isolated Enterobacter asburiae strain JCM6051 from industrial effluent of Uttarakhand regions*. 10(2): p. 64–72. https://doi.org/10.7324/JABB.2022.10s206

31. Piñon-Espitia M et al (2023) *Charge transfer effects and O2-vacancies in pure CuO nanofibers and enriched with 3.0% Mn* 295: p. 126989. https://doi.org/10.1016/j.matchemphys.2022.126989
32. Sarkodie B et al (2022) *Photocatalytic degradation of dyes by novel electrospun nanofibers: A review* : p. 137654. https://doi.org/10.1016/j.chemosphere.2022.137654
33. Eslami A et al (2018) *Application of nanosilica-based adsorbent for the removal of rhodamine B and methylene blue from aqueous solutions*. 108: p. 345–352. https://doi.org/10.5004/dwt.2018.21966
34. Hasanpour M, Motahari S, Jing D, Hatami MJTiC (2021) *Investigation of the different morphologies of zinc oxide (ZnO) in cellulose/ZnO hybrid aerogel on the photocatalytic degradation efficiency of methyl orange*. : p. 1–14. https://doi.org/10.1007/s11244-021-01476-3
35. Fotsing PN et al (2021) *Investigation of chromate and nitrate removal by adsorption at the surface of an amine-modified cocoa shell adsorbent* 9(1): p. 104618. https://doi.org/10.1016/j.jece.2020.104618
36. Fakhry H et al (2022) *Novel fabricated low-cost hybrid polyacrylonitrile/polyvinylpyrrolidone coated polyurethane foam (PAN/PVP@ PUF) membrane for the decolorization of cationic and anionic dyes*. 315: p. 115128. https://doi.org/10.1016/j.jenvman.2022.115128
37. da Farias C (2020) R.M., *Green synthesis of porous N-Carbon/Silica nanofibers by solution blow spinning and evaluation of their efficiency in dye adsorption*. 9(3): p. 3038–3046. https://doi.org/10.1016/j.jmrt.2020.01.034
38. Zhang R, Wan W, Qiu L, Zhou YJML (2016) *Facile synthesis route for MoS2-polyvinylpyrrolidone aerogels* 181: p. 321–324. https://doi.org/10.1016/j.matlet.2016.06.062
39. Silvia L, Mughayyirah Y, Zainuri M (2023) Surface modification of SiO2-based methyltrimethoxysilane (MTMS) using cetyltrimethyl ammonium bromide (CTAB) on the wettability effects through hierarchical structure. J Solgel Sci Technol 1–9. https://doi.org/10.1007/s10971-023-06202-x
40. Tepekiran BN et al (2019) *Centrifugally spun silica (SiO2) nanofibers for high-temperature air filtration*. 53(8): p. 921–932. https://doi.org/10.1080/02786826.2019.1613514
41. Khashij M et al (2020) *Removal of reactive black 5 dye using zero valent iron nanoparticles produced by a novel green synthesis method*. 49(3): p. 215–221. https://doi.org/10.1108/PRT-10-2019-0092
42. Al Akoumy C, Augé Al, Ma D, Y.J.A.A.N M, Zhao (2022) *Yolk–Shell Nanoparticles with CO2-Responsive outer shells for gas-controlled catalysis*. 5(12): p. 18237–18246. https://doi.org/10.1021/acsanm.2c04121
43. Khashij M et al (2022) *Recycled PET/metal oxides nanocomposite membrane for treatment of real industrial effluents: membrane fabrication, stability, antifouling behavior, and process modeling and optimization*. 364: p. 119966. https://doi.org/10.1016/j.molliq.2022.119966
44. Ruggiero L et al (2020) *Synthesis and characterization of TEOS coating added with innovative antifouling silica nanocontainers and TiO2 nanoparticles*. 7: p. 185. https://doi.org/10.3389/fmats.2020.00185
45. Ma D et al (2022) *Enhanced catalytic ozonation for eliminating CH3SH via stable and circular electronic metal–support interactions of Si–O–Mn bonds with low mn loading*. 56(6): p. 3678–3688. https://doi.org/10.1021/acs.est.1c07065
46. Farias RMdC et al (2020) Green synthesis of porous N-Carbon/Silica nanofibers by solution blow spinning and evaluation of their efficiency in dye adsorption. J Mater Res Technol 9(3):3038–3046. https://doi.org/10.1016/j.jmrt.2020.01.034
47. Chen Z, Li J, Zhou J, Chen X (2023) Photothermal Janus PPy-SiO2@ PAN/F-SiO2@ PVDF-HFP membrane for high-efficient, low energy and stable desalination through solar membrane distillation. Chem Eng J 451:138473. https://doi.org/10.1016/j.cej.2022.138473
48. Liu T et al (2020) Characterization of structure and properties of MgO-Al2O3-SiO2-B2O3-Cr2O3 glass-ceramics. J Non-cryst Solids 543:120154. https://doi.org/10.1016/j.jnoncrysol.2020.120154
49. Hasanpour M, Hatami MJAiC, Science I (2020) *Application of three dimensional porous aerogels as adsorbent for removal of heavy metal ions from water/wastewater: a review study*. 284: p. 102247. https://doi.org/10.1016/j.cis.2020.102247
50. Vidovix TB et al (2022) *Efficient performance of copper oxide nanoparticles synthesized with pomegranate leaf extract for neutral red dye adsorption*. 41(5): p. e13864. https://doi.org/10.1002/ep.13864
51. Kazi SK et al (2022) *Effect of embedding aluminium and yttrium on the magneto-optic properties of lanthanum spinel ferrite nanoparticles synthesised for photocatalytic degradation of methyl red*. 104(2): p. 354–364. https://doi.org/10.1007/s10971-022-05951-5
52. Takkar S et al (2022) *Biodegradation of methyl red dye by a novel actinobacterium Zhihengliuella sp. ISTPL4: kinetic studies, isotherm and biodegradation pathway*. 26: p. 102348. https://doi.org/10.1016/j.eti.2022.102348
53. Hasanpour M, Motahari S, Jing D, Hatami MJTiC (2021) *Numerical modeling for the photocatalytic degradation of methyl orange from aqueous solution using cellulose/zinc oxide hybrid aerogel: Comparison with experimental data* : p. 1–14. https://doi.org/10.1007/s11244-021-01451-y
54. Hasanpour M, Hatami MJJoML (2020) Photocatalytic performance of aerogels for organic dyes removal from wastewaters. Rev Study 309:113094. https://doi.org/10.1016/j.molliq.2020.113094
55. Mehralian M, Goodarzvand Chegini Z, Khashij MJP, Technology R (2020) *Activated carbon prepared from pistachio waste for dye adsorption: experimental and CCD-based design* 49(2): p. 136–144. https://doi.org/10.1108/PRT-06-2019-0052
56. Khan A, Naeem A, Mahmood TJK, Catalysis (2020) *Kinetic studies of methyl orange and Congo red adsorption and photocatalytic degradation onto PVP-functionalized ZnO*. 61: p. 730–739. https://doi.org/10.1134/S0023158420050055
57. Tichapondwa SM, Newman J, Kubheka OJP (2020) and P.A.B.C. Chemistry of the Earth, *Effect of TiO2 phase on the photocatalytic degradation of methylene blue dye*. 118: p. 102900. https://doi.org/10.1016/j.pce.2020.102900

Authors and Affiliations

Jabran Ahmed[1] · Safia Hassan[1] · Muhammad Faiz Ahmad[1] · Zahid Imran[2] · Syed Aminullah[1] · Ayesha Gulzar[1]

✉ Safia Hassan
safia.zahid@comsats.edu.pk

✉ Zahid Imran
zahid.imran@comsats.edu.pk

[1] Department of Chemistry, COMSATS University Islamabad, Islamabad Campus, Park Road, Chak Shahzad, Islamabad 44000, Pakistan

[2] Catalysis and Sensing Materials Group, Department of Physics, COMSATS University, Islamabad Campus, Park Road, Chak Shahzad, Islamabad, Islamabad 44000, Pakistan